AIAA JOURNAL
Vol. 47, No. 5, May 2009

Design-Oriented Thermostructural Analysis with External and Internal Radiation, Part 2: Transient Response

Manav Bhatia* and Eli Livne†
University of Washington, Seattle, Washington 98195-2400

DOI: 10.2514/1.40265

This is the second paper in a two-part series presenting a sensitivity-analysis formulation covering configuration shape and structural sizing design variables for nonlinear thermostructural analysis including the effects of radiation: external and in internal cavities. Part 1 presented the steady-state coupled thermal–structural formulation with results from a new coupled design-oriented thermoelastic analysis capability. The present paper considers transient heat transfer analysis problems with temperature-dependent material properties. Structural response is assumed to be quasi-steady. Because structural–thermal integration had been demonstrated earlier, the focus here is on design-oriented analysis aspects of the conduction–radiation problem. An approximation scheme is presented for the category of problems discussed that leads to a reduction of CPU cost from the order of N^3 operations to N^2 for cavity radiation analysis. A hypersonic wing structure similar to a space shuttle wing is used as a test case.

Nomenclature

$[A]$	=	matrix used in cavity radiation analysis, Eq. (28)
$[B]$	=	matrix used in cavity radiation analysis, Eq. (29)
$[B^k]$	=	internal radiation $[B]$ matrix at the kth iteration
$[C(T)]$	=	thermal finite element capacitance matrix
$C_p(T)$	=	material specific heat, temperature-dependent, J/kg/K
$[G]$	=	interpolation matrix for obtaining finite element nodal heat loads from cavity radiation net surface heat flux
$[G]_L$	=	interpolation matrix for a set of cavity radiation elements L, Eq. (39)
h	=	coefficient of convective heat transfer, $W/m^2/K$
$[J]$	=	Jacobian of the heat transfer finite element equations
$[K_c(T)]$	=	thermal finite element conductivity matrix
$[K_h]$	=	conductance matrix resulting from surface convection
$k(T)$	=	material isotropic thermal conductivity, temperature-dependent, W/m/K
$\{N\}$	=	finite element shape-function matrix, unique for each element kind
$\hat{n}$	=	surface normal
$\mathbf{q}$	=	surface flux on S_1 due to imposed temperatures T_s, W/m^2
$\{q_R\}$	=	vector of net radiation heat flux for all surfaces in a radiation cavity
q_{R_I}	=	incident radiation heat flux on boundary S_4, W/m^2
$\{q_{R_I}\}$	=	vector of incident radiation heat flux for all surfaces in a radiation cavity
q_{R_o}	=	radiation heat flux leaving a surface, W/m^2
$\{q_{R_o}\}$	=	vector of outgoing radiation heat flux for all surfaces in a radiation cavity
q_i	=	tensor representation of heat flux, W/m^2
q_{s_2}	=	surface heat flux applied on the boundary S_2, W/m^2
q_v	=	internal volume heat generation, W/m^3
$\{R_h\}$	=	thermal finite element nodal heat-load vector on boundary S_3, where a convection boundary condition is specified
$\{R_Q\}$	=	thermal finite element nodal heat-load vector due to volumetric heat generation
$\{R_q\}$	=	thermal finite element nodal heat-load vector on boundary S_2, where a surface heat flux is specified
$\{R_R(T)\}$	=	thermal finite element nodal heat-load vector due to internal radiation exchange on boundary S_4, where the surface participates in internal cavity radiation exchange
$\{R_T\}$	=	thermal finite element nodal heat-load vector on boundary S_1, where a temperature boundary condition is specified
$\{R_\sigma(T)\}$	=	thermal finite element nodal heat-load vector due to emitted heat radiation on boundary S_4, where a surface radiation boundary condition is specified
S_1	=	surface boundary with imposed temperature T_s
S_2	=	surface boundary with imposed heat flux q_s
S_3	=	surface boundary with imposed convection heat flux
S_4	=	surface boundary with imposed incident radiation heat flux q_{R_I}
T	=	material temperature, K
T_{abs}	=	absolute temperature scale, 273.16 K
$\tilde{T}_e$	=	average finite element temperature, calculated by averaging temperatures at nodes of an element
T_R	=	discretized temperature variable in internal cavity radiation analysis
T_{s_1}	=	temperature imposed on the surface boundary S_1, K
T_T	=	discretized temperature variable in conduction finite element analysis
$\{T_T\}$	=	thermal finite element nodal temperature vector
T_∞	=	ambient temperature, K
t	=	time, s
X	=	arbitrary design variable (shape, material, or cross-sectional size)
$\alpha_R(T)$	=	coefficient of surface thermal radiation absorptivity, temperature-dependent
Γ	=	boundary of integration domain
$\Delta\epsilon_{R_i}^k$	=	change in emissivity at the kth iteration with a reference value $\epsilon_{R_i}^0$

Received 5 August 2008; revision received 15 December 2008; accepted for publication 17 December 2008. Copyright © 2009 by M. Bhatia and E. Livne. Published by the American Institute of Aeronautics and Astronautics, Inc., with permission. Copies of this paper may be made for personal or internal use, on condition that the copier pay the $10.00 per-copy fee to the Copyright Clearance Center, Inc., 222 Rosewood Drive, Danvers, MA 01923; include the code 0001-1452/09 $10.00 in correspondence with the CCC.

*Ph.D. Student, Department of Aeronautics and Astronautics; currently Postdoctoral Fellow, Virginia Polytechnic Institute and State University, Department of Aerospace and Ocean Engineering. Member AIAA.

†Professor, Department of Aeronautics and Astronautics, Box 352400. Associate Fellow AIAA.

$\epsilon_R(T)$ = coefficient of surface thermal radiation emissivity, temperature-dependent
$\epsilon^0_{R_i}$ = emissivity of the ith surface at a reference iteration 0
$\left[\theta^k_{R_i}\right], \left[\gamma^k_{R_i}\right]$ = intermediate vectors used in approximation of $[A][B]^{-1}$ in internal radiation analysis, Eqs. (55) and (57), respectively
$\rho(T)$ = material density, temperature-dependent, $\mathrm{kg/m^3}$
σ = Stefan–Boltzmann constant, $5.670400 \times 10^8\ \mathrm{W/m^2/K^4}$
$\{\psi\}$ = intermediate vector used in cavity radiation analysis, Eq. (44)
Ω = integration domain
Ω_i = integration domain of the ith cavity radiation surface
$\{\}$ = differentiation with respect to time

Subscripts

e = element-level finite element quantity
I = incident radiation flux
i = ith index
o = emitted radiation flux

Introduction

FOR any aerospace vehicle, heat inputs and temperature distributions over the structure result in 1) generation of thermal stresses and deformations and 2) possible changes in material properties at higher operating temperatures. Thermal simulations of typical aerospace vehicles need to take into account the effect of radiation on the external boundary of the surface as well as in cavities inside the structure.

Design-oriented analysis, in the context of methods development for multidisciplinary design optimization, aims at providing accurate analysis as well as behavior sensitivity results at low computational cost relative to full-order detailed analysis. Based on analysis and sensitivity results and using intermediate design variables, intermediate response functions, and other concepts, approximation techniques are sought that would replace detailed costly analysis with efficient approximations to allow effectively carrying out large numbers of repeated analyses, which is required in any optimization search.

Much of the success of approximation techniques in the case of structural synthesis can be attributed to deep engineering insight regarding the mathematical dependency of behavior functions on design variables and the identification, taking advantage of the mathematical structure of a problem, of effective intermediate design variables and response functions.

In previous publications [1,2], a design-oriented formulation for a coupled thermal–structural analysis and sensitivity analysis of flight vehicle structures had been presented, allowing for sizing type as well as configuration shape variations. The present paper expands the work to transient cases in which material properties change with temperature. The focus here is on the conduction–radiation part of the problem. Sensitivity-analysis methodology for shape as well as material-property design variables is formulated and studied in detail to identify intermediate steps and internal dependencies in which approximation concepts can be introduced. Such approximations are indeed identified, and in a set of test studies, sensitivity results are verified, performance of the new approximations is assessed (both accuracy and computational cost), and, finally, representative analysis and sensitivity results for parametric changes in shape design variables are used in an effort to gain insight regarding relations between design variables and response functions in this particular quite complex problem. A boundary-element-based approach for combined internal radiation–conduction problem with participating medium in the cavity was presented by Dems and Korycki [3] and Korycki [4].

It is assumed here that the thermoelastic deformations of the structure do not affect the transient thermal (conduction and radiation) nature of the problem. Given that characteristic time of a transient structural response is very small, as compared with the characteristic time of the thermal response, this is a valid assumption and has been used for practically all problems relating to aerospace vehicles so far. Hence, the temperature (and its sensitivity) calculated using the formulation presented in this paper can be applied as a quasi-steady field on the structure for evaluation of various structural response quantities and their sensitivities.

Fundamental Equations

Heat-Conduction Finite Element Analysis

The governing differential equation for the time-dependent heat transfer problem is written as

$$\rho(T)C_p(T)\frac{\partial T}{\partial t} + q_{i,i} - q_v = 0 \qquad i = 1, 2, 3 \tag{1}$$

Fourier's law of heat conduction defines the relation between the heat flux and temperature gradient as

$$q_i = -(k(T)T)_{,i} \tag{2}$$

where $k(T)$ is the coefficient of thermal conductivity. Boundary conditions for this differential equation (1) can be of the following form: $T = T_{s_1}$ (temperature boundary condition on S_1), $q = q_{s_2}$ (surface heat flux on S_2), $q = -h(T - T_\infty)$ (surface heat convection on S_3), $q = -\sigma\epsilon_R(T)T^4$ (emitted radiation on S_4), and $q = \alpha_R(T)q_{R_I}$(absorbed radiation on S_4), where S_1, S_2, S_3, and S_4 belong to the boundary of the domain.

The discretized finite element equation of transient conduction heat transfer assembled for all elements is written as [5]

$$[C(T)]\{\dot{T}_T\} + [[K_c(T)] + [K_h]]\{T_T\} = \{R_T\} + \{R_Q\} + \{R_q\} + \{R_h\} + \{R_\sigma(T)\} + \{R_R(T)\} \tag{3}$$

where the global equations are assembled from element-level quantities defined as [5]

$$[C(T)]_e = \int_\Omega (\{N\}\rho(T)C_p(T)\{N\}^T)\mathrm{d}\Omega \tag{4}$$

$$[K_c(T)]_e = \int_\Omega (\{N\}_{,i}k_i(T)\{N\}^T_{,i})\mathrm{d}\Omega \tag{5}$$

$$[K_h]_e = \int_{S_3} h\{N\}\{N\}^T\mathrm{d}\Gamma \tag{6}$$

$$\{R_T\}_e = -\int_{S_1} (\mathbf{q}\cdot\hat{n})\{N\}\mathrm{d}\Gamma \tag{7}$$

$$\{R_Q\}_e = \int_\Omega q_v\{N\}\mathrm{d}\Omega \tag{8}$$

$$\{R_q\}_e = \int_{S_2} q_s\{N\}\mathrm{d}\Gamma \tag{9}$$

$$\{R_h\}_e = \int_{S_3} hT_\infty\{N\}\mathrm{d}\Gamma \tag{10}$$

$$\{R_\sigma(T)\}_e = -\int_{S_4} \sigma(\epsilon_R(T)(\{N\}^T\{T_T\}_e + T_{\text{abs}})^4 - \alpha_R(T)(T_\infty + T_{\text{abs}})^4)\{N\}\mathrm{d}\Gamma \tag{11}$$

The load vector $\{R_R(T)\}$ is obtained from a cavity radiation analysis, which is presented in a later section in this paper, resulting in Eq. (40). Because material properties depend on temperature, they vary over the domain of integration for each finite element. This means that for accuracy, material properties should be evaluated at each finite element quadrature point using the temperature at that point. Design-oriented-analysis capabilities focus on, in addition to analysis accuracy, effective sensitivities and approximations, together with the low computational costs required for the rapid reanalyses required for incorporation into multidisciplinary design optimization capabilities. For the design-oriented formulation presented here, the formulation and results reported are based on using material properties that are calculated at the *average nodal* temperature for each element and are hence constant over the domain of an element. Hence, the material properties vary from one element to another, but are assumed to be constant over an individual element. The effect of this approach on the accuracy of the overall solution will depend on 1) temperature gradients over the analysis domain, 2) sensitivity of material properties with respect to temperature, and 3) element mesh density in the analysis domain. A few notes about the averaging of material properties in a design-oriented analysis approach over individual elements are in order.

The finite element matrices for thermal analysis are calculated (in a general form) by numerical quadrature as

$$\sum_q \left(\frac{\partial\{N\}}{\partial x_i} k(T) \frac{\partial\{N\}^T}{\partial x_i}\right)_q$$

where i is the ith coordinate axis, and q are the indices over the quadrature points. If the material properties are assumed to be constant over an element's domain, then this expression can be simplified to

$$k\sum_q \left(\frac{\partial\{N\}}{\partial x_i} \frac{\partial\{N\}^T}{\partial x_i}\right)_q$$

The conductivity $k(T)$ can now be calculated only for one average temperature value. Additionally, the summed-up quantity (which is only a geometrical quantity) can be calculated once and saved for future reference. In the case of nonlinear analysis, in which the conductance matrix is to be calculated at each iteration or in which multiple load cases are solved, this matrix can be quickly recovered, multiplied by a factor, and added to the global matrix. Sensitivity with respect to material property can be easily calculated, in which the stored matrix only has to be multiplied by a simple factor. This matrix is used directly for semi-analytic shape sensitivity with finite difference. For coupling the finite element conduction and internal cavity radiation meshes, the expression

$$\epsilon_{R_i}(T_{R_i})A_{R_i}(T_{R_i} + T_{\text{abs}})^4 = \int_{\Omega_i} \epsilon_{R_i}(T_T)(\{N\}^T\{T_T\} + T_{\text{abs}})^4\mathrm{d}\Omega$$

defines the relation between temperature on a conduction mesh to temperature on a radiation mesh. (This is the same as Eq. (33) presented later in this paper.) In this analysis, it is assumed that the conduction and radiation analysis share the same physical properties [i.e., $\epsilon_{R_i}(T_{R_i}) = \epsilon_{R_i}(T_T)$], which are assumed to be constant over the domain of each element. This allows the equation to be simplified to

$$(T_{R_i} + T_{\text{abs}})^4 = \frac{1}{A_{R_i}} \int_{\Omega_i} (\{N\}^T\{T_T\} + T_{\text{abs}})^4\mathrm{d}\Omega$$

which defines the expression for temperature on the radiation mesh. Details about this procedure are presented in a subsequent section on combined radiation–conduction analysis formulation.

The nonlinear transient system of equations (3) is solved using Newmark's method [6]. The solution process requires calculation of a Jacobian matrix, which is defined as

$$[J_{ij}] = \frac{\partial([C(T)_{il}]\{\dot{T}_{T_l}\} + [K_c(T)_{il}]\{T_{T_l}\} - \{R_\sigma(T)_i\} - \{R_R(T)_i\})}{\partial\{T_{T_j}\}} \tag{12}$$

where these global quantities are assembled from element-level quantities defined as

$$\frac{\partial([C(T)_{il}]\{\dot{T}_{T_l}\})_e}{\partial\{T_{T_j}\}_e} = \left[\frac{\partial C(T)_{il}}{\partial T_{T_j}} \dot{T}_{T_l}\right]_e \tag{13}$$

$$\frac{\partial([K_c(T)_{il}]\{T_{T_l}\})_e}{\partial\{T_{T_j}\}_e} = [K_c(T)_{ij}]_e + \left[\frac{\partial K_c(T)_{il}}{\partial T_{T_j}} T_{T_l}\right]_e \tag{14}$$

$$\frac{\partial\{R_\sigma(T)\}_e}{\partial\{T_T\}_e} = -\int_{S_4} \sigma\left(\frac{\partial\epsilon_R(T)}{\partial T}(\{N\}^T\{T_T\}_e + T_{\text{abs}})^4 + 4\epsilon_R(T)(\{N\}^T\{T_T\}_e + T_{\text{abs}})^3 - \frac{\partial\alpha_R(T)}{\partial T}(T_\infty + T_{\text{abs}})^4\right)\{N\}\{N\}^T\mathrm{d}\Gamma \tag{15}$$

where repeated indices indicate summation over the index. The last term in Eq. (12) is calculated from cavity radiation analysis, which is presented in the next section.

Sensitivity Analysis

The semi-analytic sensitivity-analysis method is used in this work [7]. A general set of nonlinear first-order ordinary differential equations at time t can be written in residual form as

$$\{r(t, X, \{\dot{u}\}, \{u\})\} = 0 \tag{16}$$

where the residual $\{r\}$ is defined as

$$\{r(t, X, \{\dot{u}\}, \{u\})\} = [C(t, X, \{u\})]\{\dot{u}(t, X)\} + [K(t, X, \{u\})]\{u(t, X)\} - \{R(t, X, \{u\})\} \tag{17}$$

The sensitivity equations can be obtained by implicitly differentiating Eq. (16) with respect to the design variable X to obtain

$$\frac{\partial\{r\}}{\partial\{\dot{u}\}} \frac{\partial\{\dot{u}\}}{\partial X} + \frac{\partial\{r\}}{\partial\{u\}} \frac{\partial\{u\}}{\partial X} + \frac{\partial\{r\}}{\partial X} = 0 \tag{18}$$

For the case of thermal-conduction sensitivity analysis, this can be written as

$$[C(t, X, T)]\frac{\partial\{\dot{T}\}}{\partial X} + [J_{ij}]\frac{\partial\{T\}}{\partial X} = -\frac{\partial[C(t, X, \{T\})]}{\partial X}\{\dot{T}\} - \frac{\partial[K(t, X, \{T\})]}{\partial X}\{T\} + \frac{\partial\{R(t, X, \{T\})\}}{\partial X} \tag{19}$$

This is a linear ordinary differential equation with the solution sensitivity terms $\partial\{\dot{T}\}/\partial X$ and $\partial\{T\}/\partial X$ as the unknown variables. Once the solution to Eq. (16) is available, the calculated solution and stored Jacobians $[J_{ij}]$ are used to solve the sensitivity equation (18) using a linear time-integration scheme.

Relating Eqs. (3), (16), and (19), the solution will require the sensitivity of the element matrices and vectors, which are calculated

as follows:

$$\frac{\partial[C(T)]_e}{\partial X} = \frac{\partial(\rho(\tilde{T}_e)C_p(\tilde{T}_e))}{\partial X}\int_\Omega \{N\}\{N\}^T \mathrm{d}\Omega + (\rho(\tilde{T}_e)C_p(\tilde{T}_e))\frac{\partial\left(\int_\Omega \{N\}\{N\}^T \mathrm{d}\Omega\right)}{\partial X} \tag{20}$$

$$\frac{\partial[K_c(T)]_e}{\partial X} = \frac{\partial k_i(\tilde{T}_e)}{\partial X}\int_\Omega \{N\}_{,i}\{N\}_{,i}^T \mathrm{d}\Omega + k_i(\tilde{T}_e)\frac{\partial\left(\int_\Omega \{N\}_{,i}\{N\}_{,i}^T \mathrm{d}\Omega\right)}{\partial X} \tag{21}$$

$$\frac{\partial[K_h]_e}{\partial X} = \frac{\partial h}{\partial X}\int_{S_3} \{N\}\{N\}^T \mathrm{d}\Gamma + h\frac{\partial\left(\int_{S_3} \{N\}\{N\}^T \mathrm{d}\Gamma\right)}{\partial X} \tag{22}$$

$$\frac{\partial\{R_Q\}_e}{\partial X} = \frac{\partial q_v}{\partial X}\int_\Omega \{N\}\mathrm{d}\Omega + q_v\frac{\partial\left(\int_\Omega \{N\}\mathrm{d}\Omega\right)}{\partial X} \tag{23}$$

$$\frac{\partial\{R_q\}_e}{\partial X} = \frac{\partial q_s}{\partial X}\int_{S_2} \{N\}\mathrm{d}\Gamma + q_s\frac{\partial\left(\int_{S_2} \{N\}\mathrm{d}\Gamma\right)}{\partial X} \tag{24}$$

$$\frac{\partial\{R_h\}_e}{\partial X} = \frac{\partial(hT_\infty)}{\partial X}\int_{S_3} \{N\}\mathrm{d}\Gamma + hT_\infty\frac{\partial\left(\int_{S_3} \{N\}\mathrm{d}\Gamma\right)}{\partial X} \tag{25}$$

$$\frac{\partial\{R_\sigma(T)\}_e}{\partial X} = -\sigma\frac{\partial\epsilon_R(\tilde{T}_e)}{\partial X}\int_{S_4} (\{N\}^T\{T_T\}_e + T_{\text{abs}})^4\{N\}\mathrm{d}\Gamma - \sigma\epsilon_R(\tilde{T}_e)\frac{\partial\left(\int_{S_4}(\{N\}^T\{T_T\}_e + T_{\text{abs}}\right)^4\{N\}\mathrm{d}\Gamma)}{\partial X} + \sigma\frac{\partial(\alpha_R(\tilde{T}_e)(T_\infty + T_{\text{abs}})^4)}{\partial X}\int_{S_4}\{N\}\mathrm{d}\Gamma + \sigma(\alpha_R(\tilde{T}_e)(T_\infty + T_{\text{abs}})^4)\frac{\partial\left(\int_{S_4}\{N\}\mathrm{d}\Gamma\right)}{\partial X} \tag{26}$$

where X is the design parameter, which can be a material, shape, or element cross-sectional property. The details for calculation of $\partial\{R_R(T)\}/\partial X$ are presented in the next section on internal radiation. All quantities involving the shape functions are purely geometric in nature and are calculated using finite difference. All material properties are calculated at the element average temperature $\tilde{T}_e$. For load vectors, the sensitivity of loads can be a nonzero quantity for multidisciplinary problems and needs to be accounted for. For example, in an aerothermodynamic simulation, a shape change of the vehicle can lead to a change in the surface heat flux, implying that the sensitivity of the load with respect to the design parameter ($\partial q_s/\partial X$) can be a nonzero quantity.

Cavity Radiation

Details of cavity radiation analysis with constant material properties can be found in part 1 of this paper [1]. In this section, those equations that change due to temperature-dependent properties are presented. The discretized equations for cavity radiation analysis can be written as

$$\begin{Bmatrix}\{q_R\}\\ \{q_{R_i}\}\\ \{q_{R_o}\}\end{Bmatrix} = \begin{Bmatrix}[A][B]^{-1}\{(T_R + T_{\text{abs}})^4\}\\ \sigma[F_{i-j}][B]^{-1}\{(T_R + T_{\text{abs}})^4\}\\ \sigma[B]^{-1}\{(T_R + T_{\text{abs}})^4\}\end{Bmatrix} \tag{27}$$

where

$$[A] = \sigma[[I] - [F_{i-j}]] \tag{28}$$

$$[B] = \left[\left[\frac{1}{\epsilon_R(T)}\right]_{\text{diag}} - \left[\frac{1-\epsilon_R(T)}{\epsilon_R(T)}\right]_{\text{diag}}[F_{i-j}]\right] \tag{29}$$

The matrix $[B]$ is dependent on temperature, due to temperature dependence of the emissivity ϵ_R.

Combined Conduction Finite Element and Internal Cavity Radiation Analysis

Analysis Formulation

Both the conduction heat transfer finite element analysis and the internal cavity radiation analysis have their own computational meshes, with individual definitions of unknown variables and loads. Hence, for a combined analysis, a consistent approach has to be followed to couple the two disciplines. The details of this coupling are presented in [1] for the case of constant material properties. A similar process of energy balance is used to convert the conduction finite element nodal temperatures to the cavity radiation surface temperatures and to convert the cavity radiation surface heat flux to a conduction finite element nodal heat-load vector.

A radiation cavity is defined by specifying the enclosing conduction finite element faces that participate in radiation exchanges. These will now be referred to as *radiation faces* (i.e., the faces of conduction finite elements that participate in internal cavity radiation). For 2-D elements, a radiation face is defined by its integration domain, and each face of a 3-D element can act as a radiation face.

Once a cavity has been defined in this manner, the isothermal cavity radiation elements are defined by subdivision of the radiation faces. For example, in Fig. 1, a 4-node quadrilateral conduction finite element defined by the four nodes G1, G2, G3, and G4 has been subdivided into 4 cavity radiation elements: R1, R2, R3, and R4.

Let T_{R_i} be the temperature of the ith cavity radiation element, and let $\{T_T\}_i$ be a vector of nodal temperatures of the corresponding radiation face. Then T_{R_i} can be obtained by equating expressions for the radiation energy leaving the surface of cavity radiation element i. The amount of radiative energy leaving the isothermal surface is

$$q_{R_I} = \sigma\epsilon_{R_i}(T_{R_i})A_{R_i}(T_{R_i} + T_{\text{abs}})^4 \tag{30}$$

The same quantity can be calculated using conduction finite element nodal temperatures, as

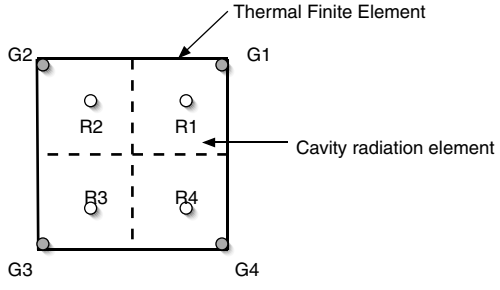

Fig. 1 Cavity radiation and finite element mesh.

Table 1 Material property base values at 35°C

Property	Base value
Thermal conductivity (skin)	126.709 W/m/K
Surface hemispherical emissivity (skin)	0.696768
Specific heat (skin)	864.06 J/kg/K
Density (skin)	2700.0 kg/m^3
Thermal conductivity (TPS)	0.0513241 W/m/K
Surface hemispherical emissivity (TPS)	0.86319
Specific heat (TPS)	675.494 J/kg/K
Density (TPS)	64.131 kg/m^3

$$q'_{R_i} = \sigma \int_{\Omega_i} \epsilon_{R_i}(T_T)(\{N\}^T\{T_T\}_i + T_{\text{abs}})^4 \text{d}\Omega \tag{31}$$

where the integration is performed over the domain of the ith cavity radiation element, which lies inside the radiation face. Because the two fluxes should be equal, then

$$q_{R_I} = q'_{R_i} \tag{32}$$

giving

$$\epsilon_{R_i}(T_{R_i})A_{R_i}(T_{R_i} + T_{\text{abs}})^4 = \int_{\Omega_i} \epsilon_{R_i}(T_T)(\{N\}^T\{T_T\}_i + T_{\text{abs}})^4 \text{d}\Omega \tag{33}$$

This is a nonlinear equation with T_{R_i} as the unknown variable. Because solving Eq. (33) for each cavity radiation element will prove to be very expensive, it is assumed that the material property of the cavity radiation element can be evaluated at the average nodal temperature of the radiation face. This implies that

$$\epsilon_R(T_{R_i}) = \epsilon_R(T_T) \tag{34}$$

where, due to the assumption introduced in the previous section, $\epsilon_R(T_T)$ is constant over the domain of the conduction finite element and can be factored out of the integration in Eq. (33). Using Eq. (34), Eq. (33) can be simplified to

$$(T_{R_i} + T_{\text{abs}})^4 = \frac{1}{A_{R_i}} \int_{\Omega_i} (\{N\}^T\{T_T\}_i + T_{\text{abs}})^4 \text{d}\Omega \tag{35}$$

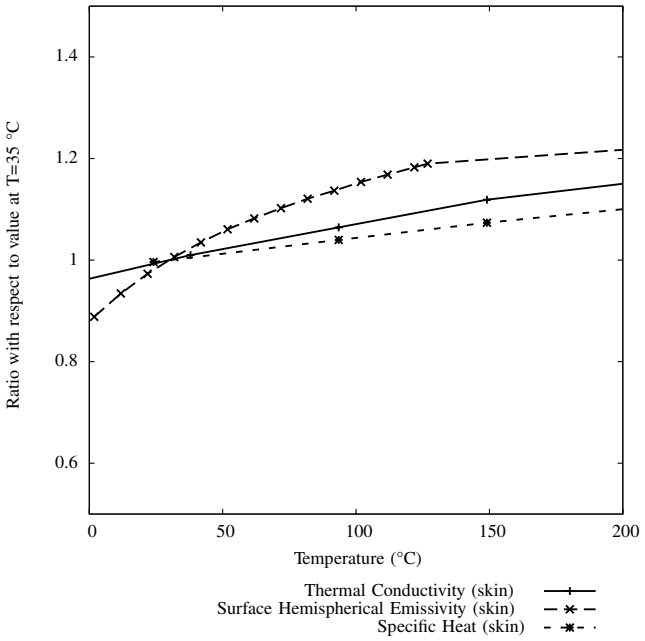

Fig. 2 Skin material-property variation with temperature shown as a ratio with respect to base property in Table 1; linear extrapolation is used outside of the temperature range shown.

This formulation attempts to differentiate between a *physical* and an *equivalent* quantity. The radiation temperatures are equivalent in the sense that they provide a consistent energy balance. However, the finite element nodal temperatures are considered to be a physical measure. Additionally, because the material of a conduction finite element and the enclosed radiation element are the same (and the material is physical in nature), it is consistent to use the same material property for the two analyses (conduction and radiation).

The basic quantity in a radiation analysis is the heat flux being emitted by a participating radiation face [$q_{\text{emitted}} = \sigma\epsilon(T_R + T_{\text{abs}})^4$]. Once q_{emitted} is available, the energy exchange due to repeated reflection, absorption, and emission is calculated by Eqs. (27).

Upon following a similar procedure for all cavity radiation elements in the cavity, the vector of temperatures $\{(T_R + T_{\text{abs}})^4)\}$ can be written as

$$\{(T_{R_i} + T_{\text{abs}})^4\} = [A_R]^{-1}_{\text{diag}} \left\{ \int_{\Omega_i} (\{N\}^T\{T_T\}_i + T_{\text{abs}})^4 \text{d}\Omega \right\} \tag{36}$$

Similarly, the net radiation flux on each cavity radiation element can be translated into a conduction finite element nodal heat-load vector. Let L be the set of all cavity radiation elements belonging to a radiation face l. Then the flux on the kth cavity radiation element q_{R_k} can be integrated over its domain Ω_k to obtain its contribution to the conduction finite element nodal heat-load vector $\{R_R\}_k$:

$$\{R_R\}_k = \int_{\Omega_k} \{N\} q_{R_k} \text{d}\Omega \tag{37}$$

where the subscript k implies a contribution due to the kth cavity radiation element. Then the total conduction finite element nodal heat load due to all cavity radiation elements in L can be obtained by summing up their contributions, giving

$$\{R_R\}_L = \left\{ \int_{\Omega_1} \{N\} q_{R_1} \text{d}\Omega + \int_{\Omega_2} \{N\} q_{R_2} \text{d}\Omega + \cdots + \int_{\Omega_N} \{N\} q_{R_N} \text{d}\Omega \right\}_L = [G]^T_L \{q_R\}_L \tag{38}$$

where $[G]_L$ is the interpolation matrix defined for cavity radiation elements in the set L, as

$$[G]_L = \begin{bmatrix} \int_{\Omega_1} \{N\}^T \text{d}\Omega \\ \int_{\Omega_2} \{N\}^T \text{d}\Omega \\ \vdots \\ \int_{\Omega_N} \{N\}^T \text{d}\Omega \end{bmatrix}_L \tag{39}$$

Using Eqs. (27) and (38) for all radiation faces in the cavity, the conduction finite element nodal heat-load vector $\{R_R\}$ can be related to nodal temperatures by

$$\{R_R\} = [G]^T[A][B]^{-1}\{(T_R + T_{\text{abs}})^4\} \tag{40}$$

where all matrices and vectors have been assembled for the entire radiation cavity. The vector $\{R_R\}$ is directly added to the conduction finite element nodal heat-load vector. The last term in Eq. (40) can be expanded using Eq. (36).

Contribution of this nonlinear nodal heat-load vector to the finite element Jacobian matrix can be calculated by differentiating Eq. (40) with respect to the conduction finite element nodal temperatures $\{T_T\}$:

$$\left[\frac{\text{d}\{R_R\}}{\text{d}\{T_T\}}\right] = [G]^T[A] \frac{\text{d}([B]^{-1}(\{T_R\} + T_{\text{abs}})^4)}{\text{d}\{T_T\}} \tag{41}$$

This involves the differentiation of a cavity radiation quantity with respect to the finite element nodal temperature vector. This can be written for a general vector [say, $p(\{T_R\})$], after chain differentiation, as

Table 2 Uniformly refined mesh for convergence study on a cubic cavity

No. of nodes	No. of elements	Relative mesh size	No. of radiation faces
26	48	0.5	48
98	192	0.25	192
386	768	0.125	768
1538	3072	0.0625	3072
6146	12,288	0.03125	——
24,578	49,152	0.015625	——
98,306	196,608	0.0078125	——

$$\left\{\frac{\mathrm{d}p(\{T_R\})}{\mathrm{d}\{T_T\}}\right\}^T = \left\{\frac{\partial p(\{T_R\})}{\partial\{T_R\}}\right\}^T \left[\frac{\partial\{T_R\}}{\partial\{T_T\}}\right] \tag{42}$$

where, from Eq. (36),

$$\left[\frac{\mathrm{d}\{T_R\}}{\mathrm{d}\{T_T\}}\right] = \frac{1}{4}[(T_R + T_{\mathrm{abs}})^3]^{-1}_{\mathrm{diag}}[A_R]^{-1}_{\mathrm{diag}} \times \left[\int_{\Omega_i} 4(\{N\}^T\{T_T\}_i + T_{\mathrm{abs}})^3\{N\}^T \mathrm{d}\Omega\right] \tag{43}$$

The last term in Eq. (41) involves differentiation of the inverse of a matrix, which is difficult to calculate. However, this problem can be simplified by rewriting this as the solution of a linear system of equations. A new vector $\{\psi\}$ is now defined so that

$$[B]\{\psi\} = \{(T_R + T_{\mathrm{abs}})^4\} \tag{44}$$

When differentiating Eq. (44) with respect to the cavity radiation temperature vector $\{T_R\}$, the left-hand side can be written in component form as

$$[\Psi_{ik}] = \frac{\partial(B_{ij}\psi_j)}{\partial T_{R_k}} = \frac{\partial B_{ij}}{\partial T_{R_k}}\psi_j + B_{ij}\frac{\partial \psi_j}{\partial T_{R_k}} = \left[\frac{\partial B_{ij}}{\partial T_{R_k}}\psi_j\right]_{\mathrm{diag}} + [B]\left[\frac{\partial \psi_j}{\partial T_{R_k}}\right] \tag{45}$$

With Eq. (44), after differentiation with respect to the cavity radiation temperature vector and using Eq. (45),

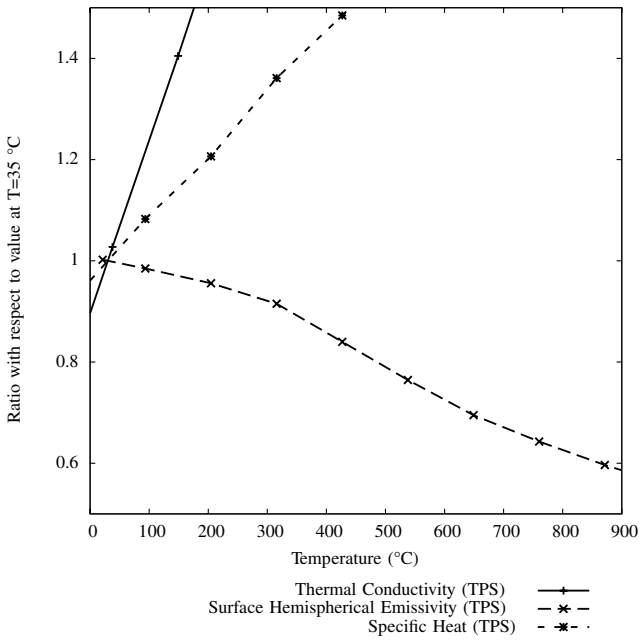

Fig. 3 TPS material-property variation with temperature shown as a ratio with respect to base property in Table 1.

$$\left[\frac{\partial \psi_i}{\partial T_{R_k}}\right] = [B]^{-1}\left(4[(T_R + T_{\mathrm{abs}})^3]_{\mathrm{diag}} - \left[\frac{\partial B_{ij}}{\partial T_{R_k}}\psi_j\right]_{\mathrm{diag}}\right) \tag{46}$$

where

$$\left[\frac{\partial B_{ij}}{\partial T_{R_k}}\psi_j\right]_{\mathrm{diag}} = \left(\left(\frac{-1}{\epsilon^2_{R_i}(T_{R_i})}\frac{\partial \epsilon_{R_i}(T_{R_i})}{\partial T_{R_k}}\delta_{ij}\delta_{ik}\right) - \left(\frac{-1}{\epsilon^2_{R_i}(T_{R_i})}\frac{\partial \epsilon_{R_i}(T_{R_i})}{\partial T_{R_k}}\delta_{il}\delta_{ik}\right)F_{lj}\right)\psi_j \tag{47}$$

is a diagonal matrix and uses the vector $\{\psi\}$ calculated using Eq. (44).

Using Eqs. (42) and (44), Eq. (41) can be written as

$$\left[\frac{\mathrm{d}\{R_R\}}{\mathrm{d}\{T_T\}}\right] = [G]^T[A]\left[\frac{\mathrm{d}\{\psi\}}{\mathrm{d}\{T_R\}}\right]\left[\frac{\partial\{T_R\}}{\partial\{T_T\}}\right] \tag{48}$$

and the last two terms in Eq. (48) can be calculated using Eqs. (43) and (46).

Sensitivity Analysis

The expression for sensitivity of $\{R_R\}$ with respect to a design variable X is obtained by differentiation of Eq. (40):

$$\frac{\partial\{R_R\}}{\partial X} = \frac{\partial([G]^T[A][B]^{-1}\{(T_R + T_{\mathrm{abs}})^4\})}{\partial X} \tag{49}$$

Using the definition of $\{\psi\}$ from Eq. (44), the sensitivity can be written as

$$\frac{\partial\{R_R\}}{\partial X} = \frac{\partial([G]^T[A]\{\psi\})}{\partial X} = \frac{\partial[G]^T}{\partial X}[A]\{\psi\} + [G]^T\frac{\partial[A]}{\partial X}\{\psi\} + [G]^T[A]\frac{\partial\{\psi\}}{\partial X} \tag{50}$$

where the sensitivity of $\{\psi\}$ can be calculated from Eq. (44) as

$$\frac{\partial\{\psi\}}{\partial X} = [B]^{-1}\left(\frac{\partial(\{(T_R + T_{\mathrm{abs}})^4\})}{\partial X} - \frac{\partial[B]}{\partial X}\{\psi\}\right) \tag{51}$$

Here, the sensitivities of $[A]$ and $[B]$ are calculated as

$$\frac{\partial[A]}{\partial X} = \sigma\frac{\partial[F_{i-j}]}{\partial X} \tag{52}$$

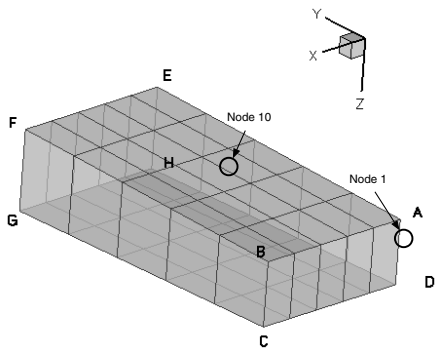

Fig. 4 Hexahedral cavity model.

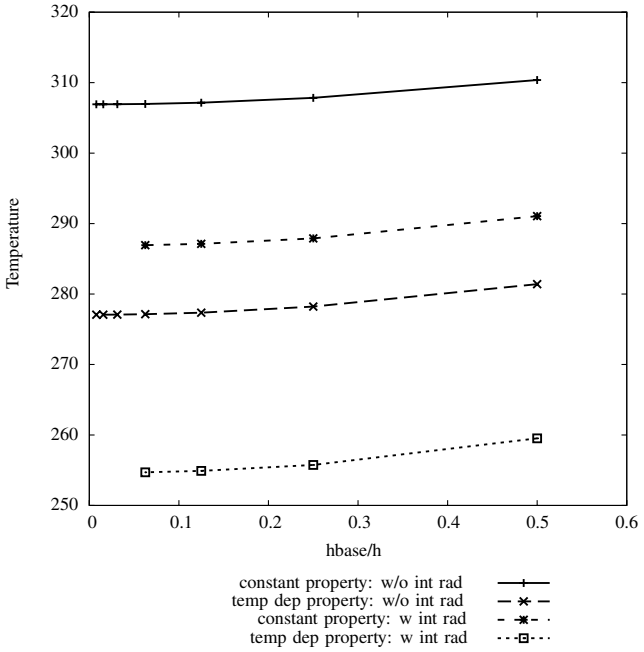

Fig. 5 Cavity nodal temperature convergence analysis over uniformly refined mesh: steady state.

$$\frac{\partial[B]}{\partial X} = \frac{\partial}{\partial X}\left(\left[\frac{1}{\epsilon_R}\right]_{\text{diag}}\right) - \frac{\partial}{\partial X}\left(\left[\frac{1-\epsilon_R}{\epsilon_R}\right]_{\text{diag}}\right)[F_{i-j}] - \left[\frac{1-\epsilon_R}{\epsilon_R}\right]_{\text{diag}} \frac{\partial[F_{i-j}]}{\partial X} \tag{53}$$

and the sensitivities of $[F_{i-j}]$, $[G]$ and $\{(T_R + T_{\text{abs}})^4)\}$ are calculated using finite differences. It must be noted that all quantities except for ϵ_R are dependent purely on geometry/shape, and hence their sensitivities will be zero for a problem in which the design variable is a material parameter or a structural sizing design variable.

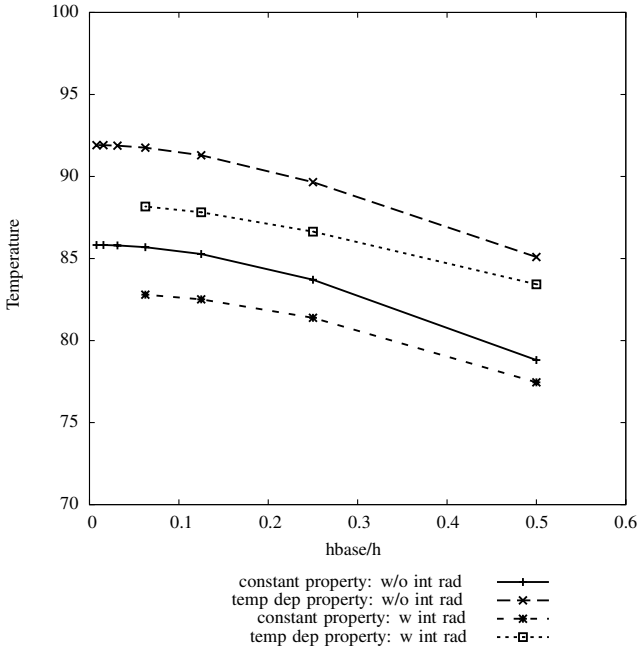

Fig. 6 Cavity nodal temperature convergence analysis over uniformly refined mesh: transient ($t = 1000$ s).

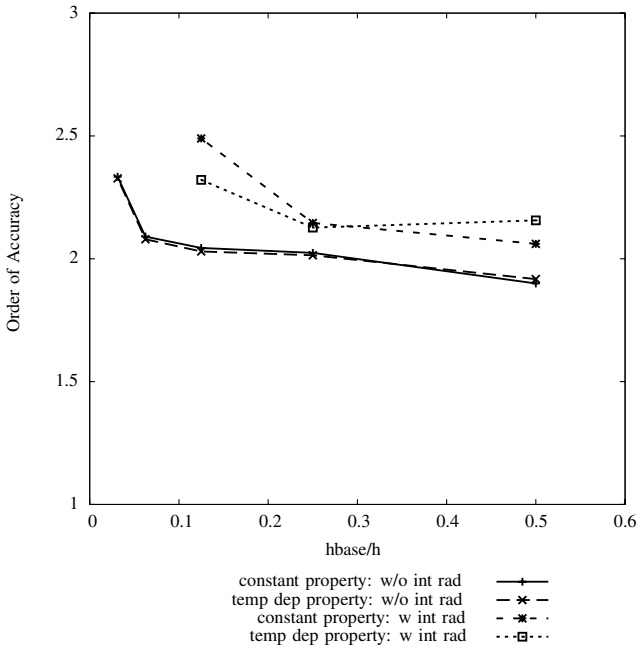

Fig. 7 Cavity nodal temperature convergence analysis over uniformly refined mesh: steady state.

Approximations

Two of the most expensive operations in the analysis considered in the paper are calculation of shape-factor matrix $[F_{i-j}]$ and inversion of $[B]$ [Eqs. (28) and (29)]. The latter becomes even more dominant for cases in which the material properties are temperature-dependent, because the matrix then has to be inverted at every nonlinear iteration. Part 1 [1] presented the idea of approximating the shape-factor matrix in a parametric analysis. Here, a new method is introduced to approximate the inverse of $[B]$. This is conceptually similar to the method introduced by Bae et al. [8], in the sense that the modifications in the matrix to be inverted are localized to specific elements and then used to approximate the new matrix. It should be noted, however, that the successive matrix inversion method [8] is an exact method and is efficient when the modifications in a matrix are

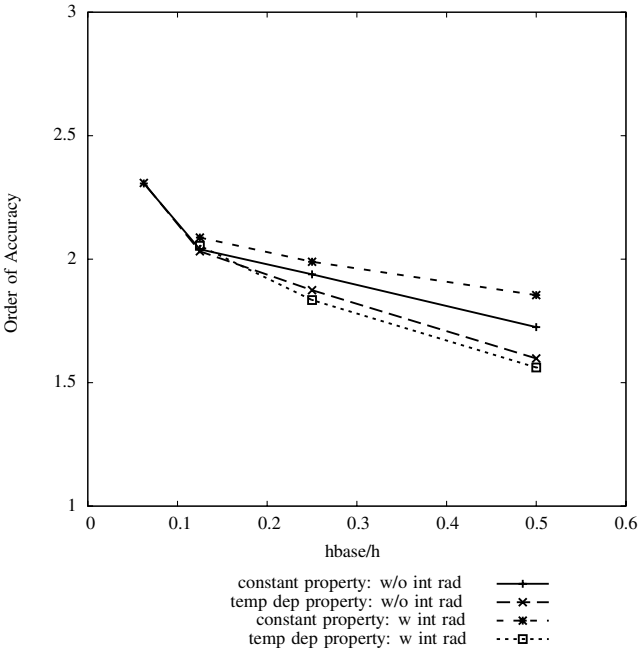

Fig. 8 Cavity nodal temperature convergence analysis over uniformly refined mesh: transient.

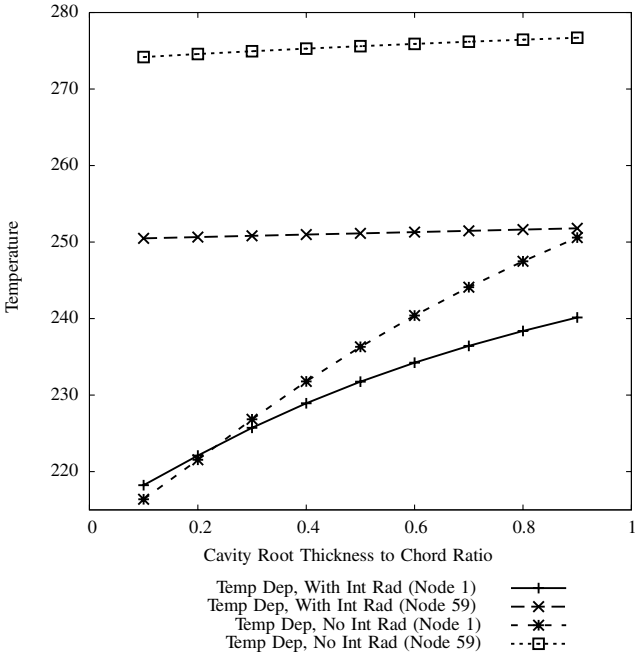

Fig. 9 Cavity nodal temperature vs t/c ratio (steady state).

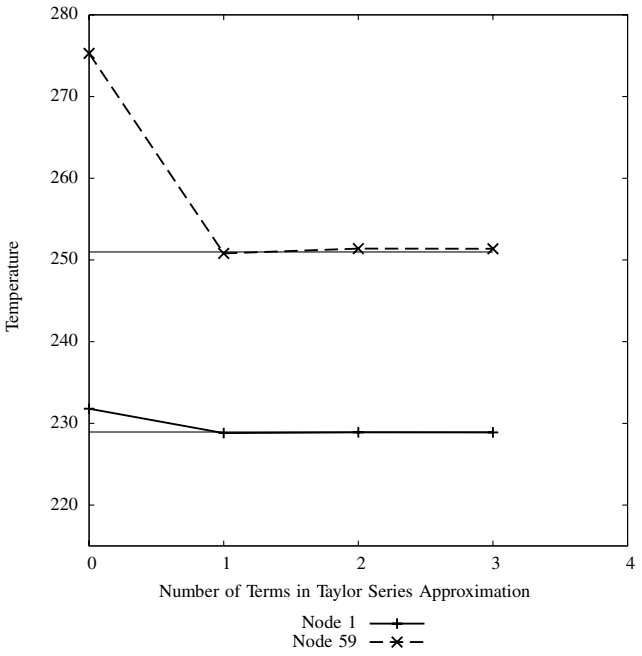

Fig. 11 Cavity nodal temperature approximation for temperature.

localized to only a few columns. Here, the modifications are localized to the diagonal of the entire matrix, and a Taylor series approximation is created.

Approximation of $[A][B]^{-1}$ Factor Matrix for Internal Radiation

Because the $[B]$ matrix is dependent on material properties, any change in material properties will require that the inverse of this matrix be recalculated in Eq. (27). For each internal radiation cavity, this will require N^3 operations per iteration of nonlinear or transient solution, which is a formidable task. It is shown here that this matrix can be approximated using the changes in material properties. The inverse can then be calculated once every predefined number of iterations and approximated for the rest.

Let $\epsilon^0_{R_i}$ be the emissivity of the ith cavity radiation surface at the beginning of the transient or nonlinear solution, and let $\Delta\epsilon^k_{R_i}$ be the change in emissivity relative to $\epsilon^0_{R_i}$ for the kth iteration. Then the matrix with these new material values at the kth iteration can be written as

$$[B^k] = \left[\frac{1}{\epsilon^0_{R_i} + \Delta\epsilon^k_{R_i}}\right]_{\text{diag}} - \left[\frac{1}{\epsilon^0_{R_i} + \Delta\epsilon^k_{R_i}} - 1\right]_{\text{diag}} [F_{i-j}] = \left[\frac{1}{\epsilon^0_{R_i}}\right]_{\text{diag}} + [\theta^k_{R_i}]_{\text{diag}} - \left(\left[\frac{1}{\epsilon^0_{R_i}} - 1\right]_{\text{diag}} + [\theta^k_{R_i}]_{\text{diag}}\right)[F_{i-j}] \tag{54}$$

where

$$\theta^k_{R_i} = -\frac{\Delta\epsilon^k_{R_i}}{\epsilon^0_{R_i}(\epsilon^0_{R_i} + \Delta\epsilon^k_{R_i})} \tag{55}$$

Equation (54) can then be rewritten as

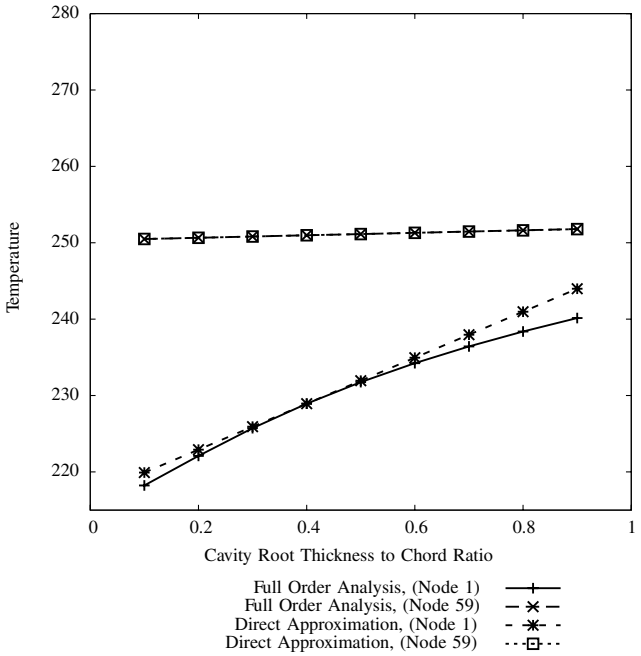

Fig. 10 Cavity nodal temperature approximation for temperature-dependent material property.

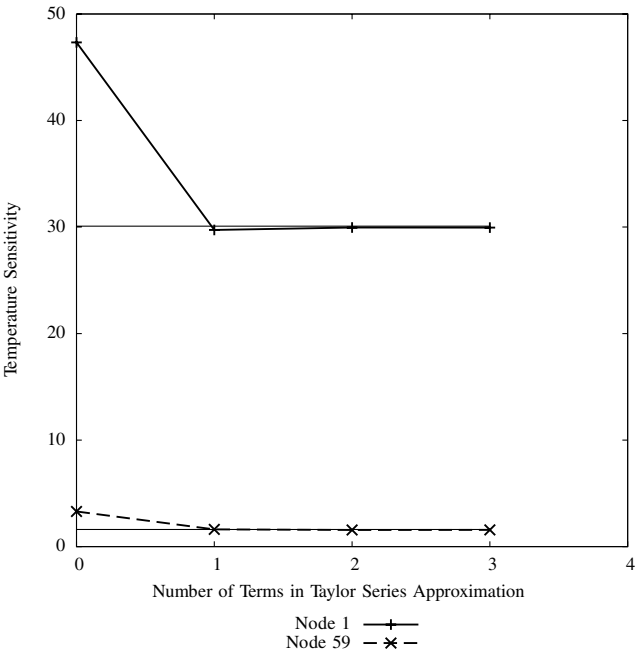

Fig. 12 Cavity nodal temperature approximation for temperature.

Table 3 Analysis times for different thermal finite element mesh densities (all values are in seconds; 1.83 GHz Intel Core Duo, 1.5 GB DDR2 SDRAM at 667 MHz running Mac OSX)

No. of radiation surfaces	$[F_{i-j}]$ time	$[A][B]^{-1}$ time	Total radiation analysis time	Total analysis time	CPU time saved
			Exact analysis		
96	0.25	0.23	0.68	1.11	——
320	2.59	2.81	6.64	7.30	——
672	10.59	27.90	44.55	46.67	——
			$[A][B]^{-1}$ *approximation with 1 term*		
96	0.25	0.03	0.43	0.57	0.53 (48.28%)
320	2.59	0.50	4.07	4.70	2.59 (35.32%)
672	10.59	3.64	19.78	21.89	24.78 (53.09%)

$$[B^k] = [B^0] + \tfrac{1}{\sigma}[\theta^k_{R_i}]_{\text{diag}}[A] \tag{56}$$

where σ is the Stefan–Boltzmann constant. The following is defined,

$$[\gamma^k_{R_i}]_{\text{diag}} = \tfrac{1}{\sigma}[\theta^k_{R_i}]_{\text{diag}} \tag{57}$$

to simplify Eq. (56) to

$$[B^k] = [B^0] + [\gamma^k_{R_i}]_{\text{diag}}[A] \tag{58}$$

Using Eq. (58), the following product is written for each iteration:

$$\begin{aligned}[A][B^k]^{-1} &= [A]([B^0] + [\gamma^k_{R_i}]_{\text{diag}}[A])^{-1} = (([B^0] \\ &+ [\gamma^k_{R_i}]_{\text{diag}}[A])[A]^{-1})^{-1} = (([A][B^0]^{-1})^{-1} \\ &+ [\gamma^k_{R_i}]_{\text{diag}})^{-1} = ([P^0] + [\gamma^k_{R_i}]_{\text{diag}})^{-1}\end{aligned} \tag{59}$$

where

$$[P^0] = ([A][B^0]^{-1})^{-1} \tag{60}$$

is calculated at the first iteration.

At any iteration, the changes in material properties are now localized to the diagonal matrix $[\gamma^k_{R_i}]_{\text{diag}}$ in Eq. (59). Treating $\gamma^k_{R_i}$ $(i = 1, \ldots, N)$ as independent variables, a Taylor series approximation for $[A][B^k]^{-1}$ can be created. In obtaining the approximation, the expression for the sensitivity of the inverse of a general matrix function $[Q(a)]$ with respect to the variable a is needed. This is obtained by first writing

$$[Q(a)]^{-1}[Q(a)] = [I] \tag{61}$$

Equation (61) can be implicitly differentiated with respect to a to obtain

$$\frac{\partial[Q(a)]^{-1}}{\partial a} = -[Q(a)]^{-1}\frac{\partial[Q(a)]}{\partial a}[Q(a)]^{-1} \tag{62}$$

$$\frac{\partial^2[Q(a)]^{-1}}{\partial a^2} = 2[Q(a)]^{-1}\frac{\partial[Q(a)]}{\partial a}[Q(a)]^{-1}\frac{\partial[Q(a)]}{\partial a}[Q(a)]^{-1} \tag{63}$$

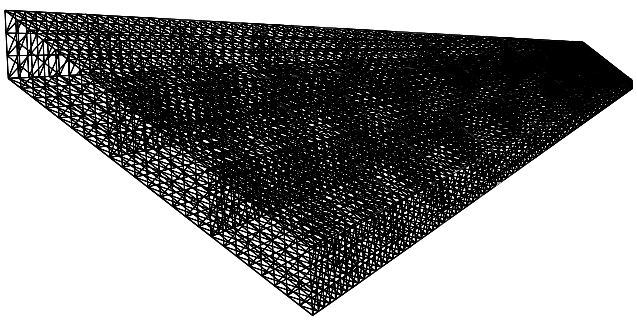

Fig. 13 Wing finite element mesh.

Table 4 Wing design variable base values

Design variable	Base value
AR	3.1
Λ_{LE}	43
c_{root}	10.2
$c_{\text{tip}}/c_{\text{root}}$	0.16
t/c_{root}	0.2

$$\begin{aligned}&\frac{\partial^3[Q(a)]^{-1}}{\partial a^3} \\ &= -6[Q(a)]^{-1}\frac{\partial[Q(a)]}{\partial a}[Q(a)]^{-1}\frac{\partial[Q(a)]}{\partial a}[Q(a)]^{-1}\frac{\partial[Q(a)]}{\partial a}[Q(a)]^{-1}\end{aligned} \tag{64}$$

Treating each diagonal term in Eq. (59) as an independent variable, Eqs. (62–64) are written for each individual term as

$$\left.\frac{\partial[S + \gamma_l\delta_{il}\delta_{jl}]^{-1}}{\partial\gamma_l}\right|_{\gamma^k=0} = -[S]^{-1}[\delta_{il}\delta_{jl}][S]^{-1} \tag{65}$$

$$\left.\frac{\partial^2[S + \gamma_l\delta_{il}\delta_{jl}]^{-1}}{\partial\gamma_l^2}\right|_{\gamma^k=0} = 2[S]^{-1}[S^{-1}_{ij}\delta_{il}\delta_{jl}][S]^{-1} \tag{66}$$

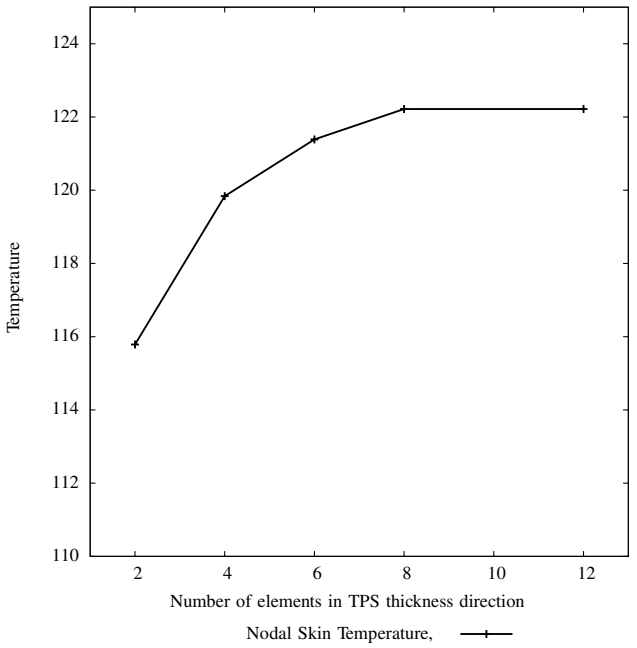

Fig. 14 Influence of number of elements along TPS thickness on the wing skin temperature.

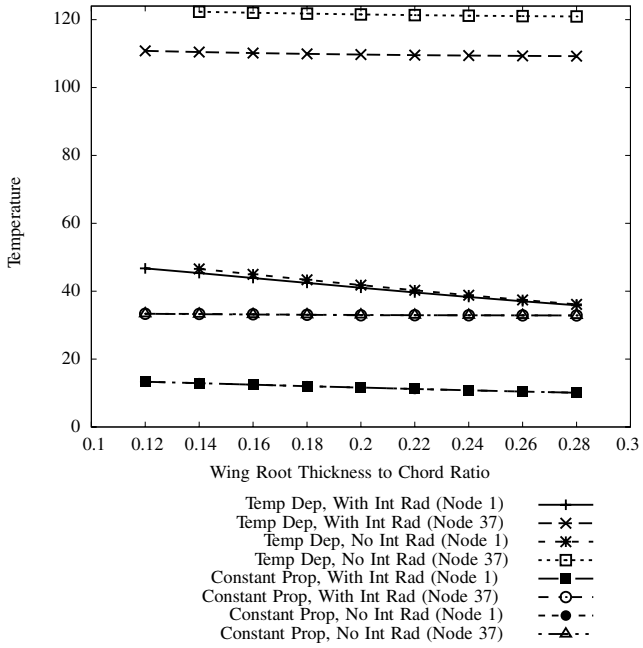

Fig. 15 Wing parametric temperature plot vs wing root thickness/ chord ratio.

$$\left.\frac{\partial^3[S+\gamma_l\delta_{il}\delta_{jl}]^{-1}}{\partial\gamma_l^3}\right|_{\gamma^k=0} = -6[S]^{-1}[S_{ij}^{-2}\delta_{il}\delta_{jl}][S]^{-1} \tag{67}$$

The following is written for the kth iteration:

$$([P^0]+[\gamma_{R_i}^k]_{\text{diag}})^{-1} = [P^0]^{-1} + \sum_{i=1}^{N}\frac{\partial([P^0]+[\gamma_{R_i}^k]_{\text{diag}})^{-1}}{\partial\gamma_{R_i}^k}\gamma_{R_i}^k + \frac{1}{2}\sum_{i=1}^{N}\frac{\partial^2([P^0]+[\gamma_{R_i}^k]_{\text{diag}})^{-1}}{\partial(\gamma_{R_i}^k)^2}(\gamma_{R_i}^k)^2+\dots \tag{68}$$

Using Eqs. (65–67), this is written in matrix form as

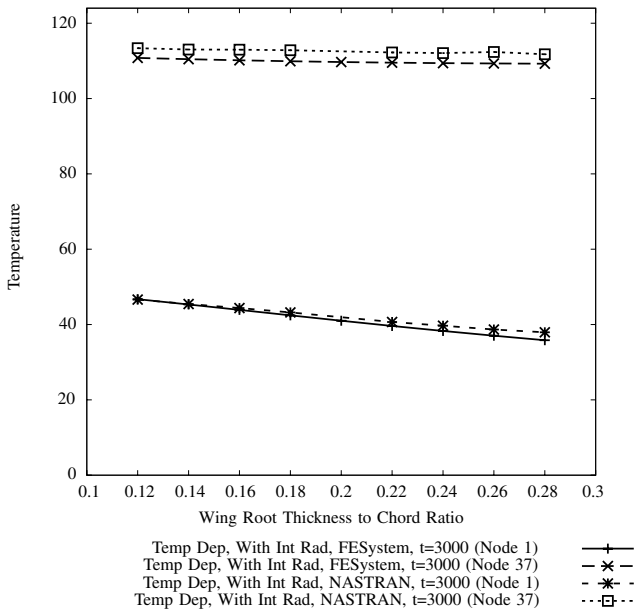

Fig. 16 Comparison of wing temperature results from FESystem and NASTRAN; temperature-dependent material properties with internal radiation.

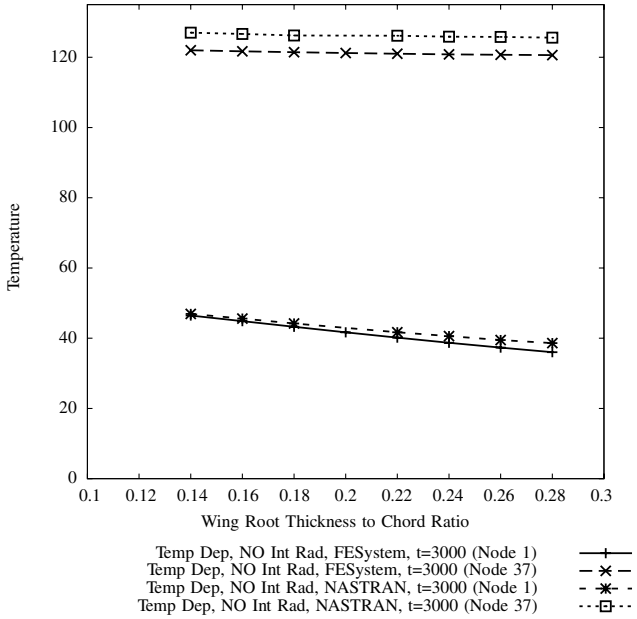

Fig. 17 Comparison of wing temperature results from FESystem and NASTRAN; temperature-dependent material properties without internal radiation.

$$([P^0]+[\gamma_{R_i}^k]_{\text{diag}})^{-1}_{\text{approx}} = [P^0]^{-1}([I]+(-[\gamma_{R_i}^k]_{diag} + [(P_{ii}^0)^{-1}(\gamma_{R_i}^k)^2]_{\text{diag}} - [(P_{ii}^0)^{-2}(\gamma_{R_i}^k)^3]_{\text{diag}}+\cdots)[P^0]^{-1}) \tag{69}$$

or in a simplified form as

$$([A][B^k]^{-1})_{\text{approx}} = [P^0]^{-1}([I]+[D^k]_{\text{diag}}[P^0]^{-1}) \tag{70}$$

where

$$[D^k]_{\text{diag}} = -[\gamma_{R_i}^k]_{\text{diag}} + [(P_{ii}^0)^{-1}(\gamma_{R_i}^k)^2]_{\text{diag}} - [(P_{ii}^0)^{-2}(\gamma_{R_i}^k)^3]_{\text{diag}}+\cdots \tag{71}$$

The matrix $[P^0]^{-1}$ is calculated once for the system and stored at the beginning of predefined number of nonlinear iterations. Then, at each

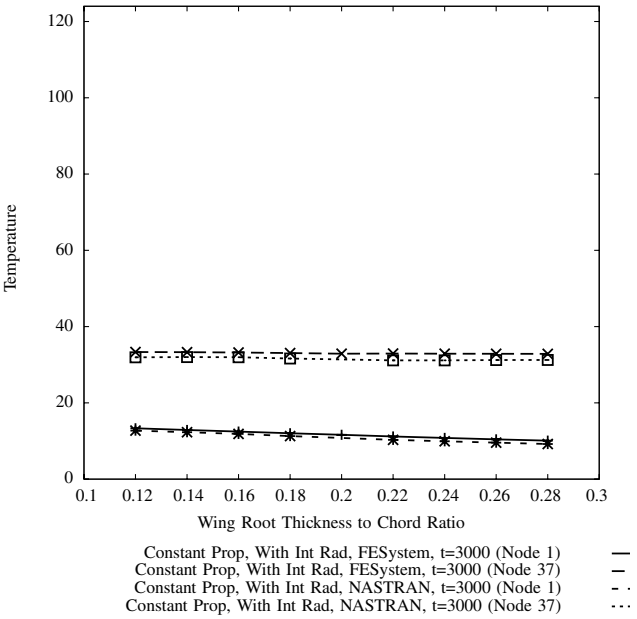

Fig. 18 Comparison of wing temperature results from FESystem and NASTRAN; temperature-independent material properties with internal radiation.

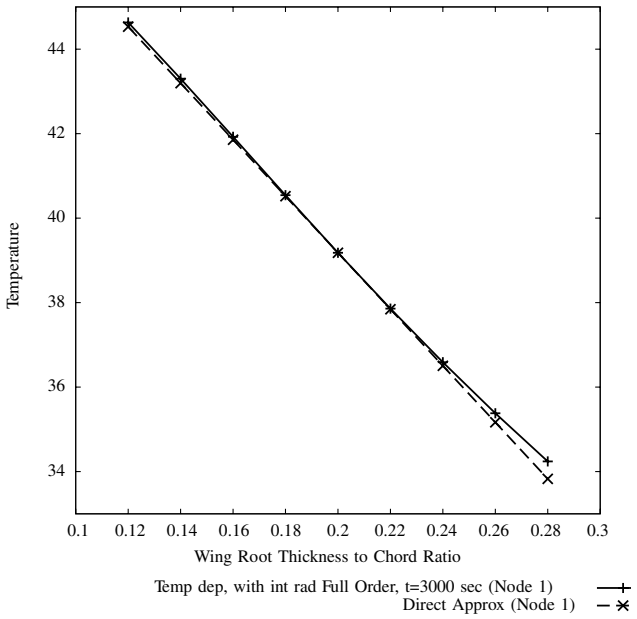

Fig. 19 Temperature approximation with sensitivity analysis (node 1); temperature-dependent material properties with internal radiation.

iteration, the diagonal matrix $[D^k]_{\text{diag}}$ is easily calculated and used, instead of inverting the $[B^k]$ matrix. This reduces the order of CPU operations from N^3 to N^2, and the CPU savings will be demonstrated in the next section. It should be noted that this approximation offers savings in radiation cavity analysis computations, and the overall savings observed in a combined conduction/cavity radiation analysis will depend on numerous other factors, such as the relative size of each system, method of time integration used, linear solvers used, etc.

The matrix product $[A][B]^{-1}$ is needed in Eqs. (27), (40), (48), and (50). In all of these equations, this matrix product is multiplied to either a vector or a diagonal matrix.

In the case of multiplication with a vector (say, $\{\lambda 0\}$), the results are efficiently obtained in three steps:

1) $\{\lambda 1\} = [P^0]^{-1}\{\lambda 0\}$

2) $\{\lambda 2\} = [D^k]_{\text{diag}}\{\lambda 1\}$

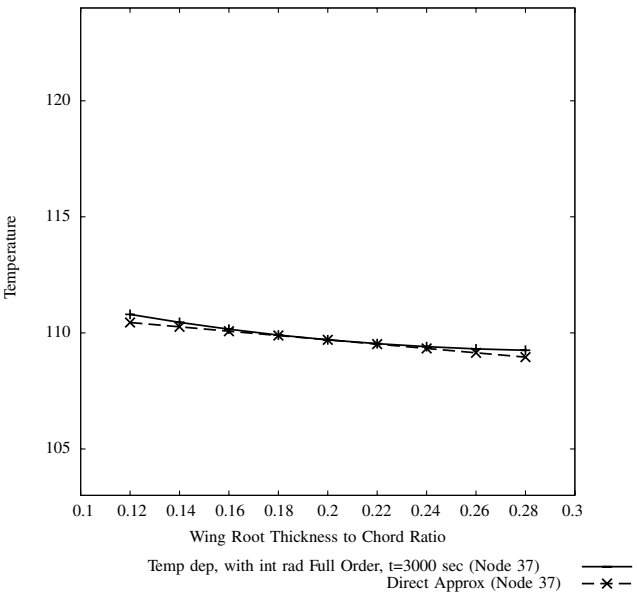

Fig. 20 Temperature approximation with sensitivity analysis (node 37); temperature-dependent material properties with internal radiation.

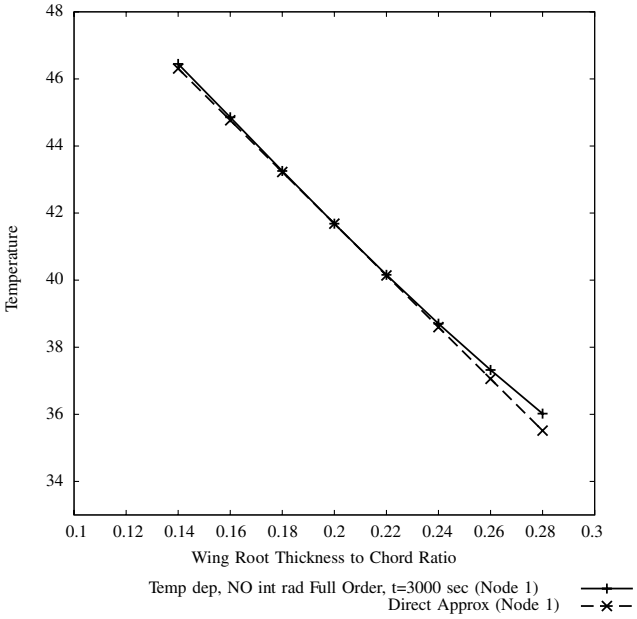

Fig. 21 Temperature approximation with sensitivity analysis (node 1); temperature-independent material properties without internal radiation.

3) $\{\lambda 3\} = \{\lambda 1\} + [P^0]^{-1}\{\lambda 2\}$

The multiplication with a diagonal matrix occurs for Jacobian calculations [Eq. (46)]. This presents a challenge because the approximation for a general diagonal matrix $[\Omega]_{\text{diag}}$ becomes

$$\begin{aligned}([A][B^k]^{-1})_{\text{approx}} &= [P^0]^{-1}([I] + [D^k]_{\text{diag}}[P^0]^{-1})[\Omega]_{\text{diag}} \\ &= [P^0]^{-1}[\Omega]_{\text{diag}} + [P^0]^{-1}[D^k]_{\text{diag}}[P^0]^{-1}[\Omega]_{\text{diag}} \end{aligned} \tag{72}$$

The last term in Eq. (72) requires a costly matrix–matrix multiplication, which reduces the advantage of this approximation because it replaces one N^3 operation by another. For this problem, however, the second term is essentially a flux-Jacobian correction and can be approximated by neglecting the offdiagonal terms as follows:

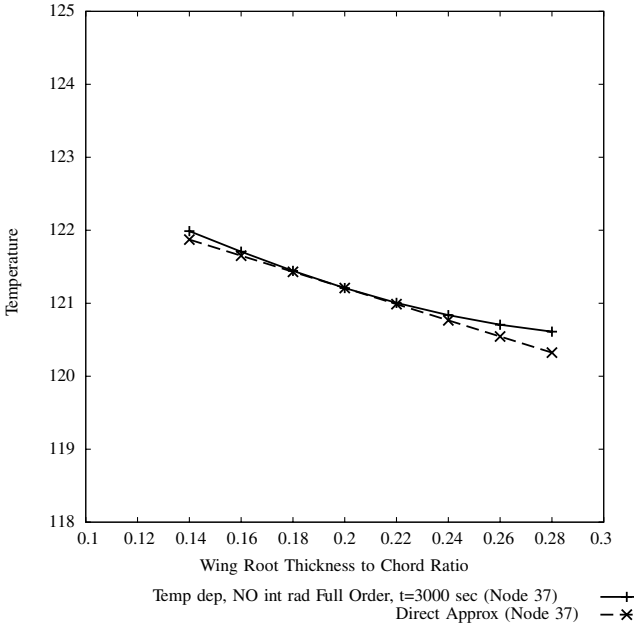

Fig. 22 Temperature approximation with sensitivity analysis (node 37); temperature-independent material properties without internal radiation.

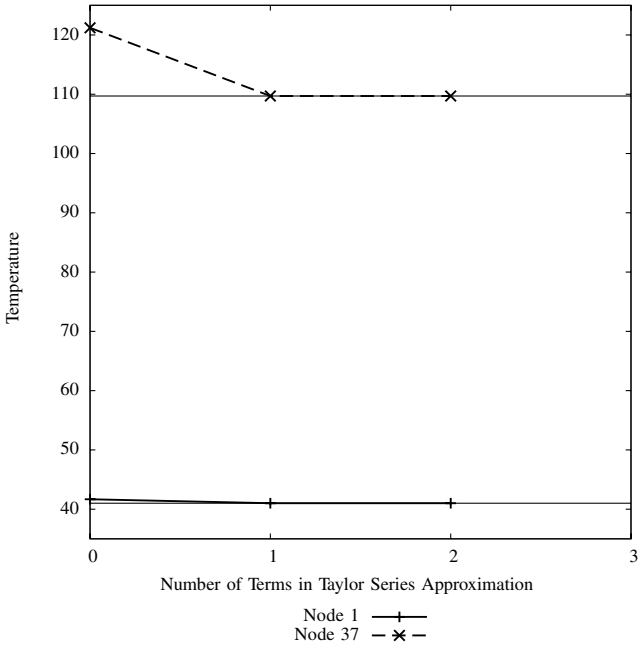

Fig. 23 Wing nodal temperature approximation for temperature.

$$([A][B^k]^{-1})_{\text{approx}} = [P^0]^{-1}[\Omega]_{\text{diag}} + [P^0]^{-1}[D^k]_{\text{diag}}([P^0]^{-1})_{\text{diag}}[\Omega]_{\text{diag}} \tag{73}$$

The offdiagonal terms represent the effect of correction in a flux Jacobian due to reflection and absorption, which is negligible in comparison with the diagonal correction terms that account for emission from a surface. Using Eq. (73), the matrix approximations are performed in two steps:

1) $[\Lambda 1]_{\text{diag}} = [D^k]_{\text{diag}}([P^0]^{-1})_{\text{diag}}[\Omega]_{\text{diag}}$

2) $[\Lambda 2] = [P^0]^{-1}([\Omega]_{\text{diag}} + [\Lambda 1]_{\text{diag}})$

When this approximation method is used, the factor $[A][B]^{-1}$ is approximated at each nonlinear iteration, as a result of which, the matrix $[B]^{-1}$ is not available. The inverse of $[B]$ is needed in Eqs. (46) and (51) for calculation of the intermediate vectors. This can be achieved by rewriting the equation for some arbitrary vectors $\{\Psi\}$ and $\{\Theta\}$ as

$$\{\Psi\} = [B]^{-1}\{\Theta\} = [A]^{-1}([A][B]^{-1})\{\Theta\} \tag{74}$$

Here, the factor $[A][B]^{-1}$ can be approximated as described earlier, and the inverse of $[A]$ can be calculated and stored at the beginning of the nonlinear iterations. The advantage of this method is that $[A]$ is dependent only on the geometry of the cavity, and hence, as long as the cavity is assumed to be nondeforming, its inverse needs to be calculated only once.

Sensitivity Analysis

Equations (70) and (74) can be used to obtain a solution of the nonlinear heat transfer equations. Once this is available, the formulation presented in the previous section can be used to obtain the sensitivity of nodal temperatures. The $[B^{-1}]$ matrix and $[A][B]^{-1}$ matrix product needed in Eqs. (49) and (51) to perform the sensitivity analysis are already available from the analysis approximations, and the sensitivity of the $[B]$ matrix can be calculated using Eq. (53).

Results and Discussion

Two examples are presented: a hexahedral cavity and a wing box with 21 internal radiation cavities. The material properties used in these two examples are shown in Table 1 and Figs. 2 and 3. The loading and results are discussed in the following.

Hexahedral Radiating Cavity: Order of Accuracy and Approximation Performance

A sample geometry of the cavity studied here is shown in Fig. 4. This is a combined conduction/radiation problem used to verify the order of accuracy of the formulation presented here in both steady-state and transient analyses. Following this, the problem is used to test the approximation presented in the previous section for a steady-state problem. A transient analysis case will be presented for a wing box in the next section. The material properties used for this analysis are shown in Table 1, and Fig. 2.

A uniform heat load of 5 kW/m^2 is applied on the bottom surface, and both the bottom and top surfaces are allowed to radiate externally. Walls of the cavity are conducting and inside the cavity all surfaces exchange heat through radiation.

For numerical verification of the order of accuracy, each dimension of the cavity is fixed to the unit value (hollow cube), and steady-state and transient simulations (for 1000 s) are performed for uniformly refined mesh. The details of the mesh are given in Table 2. Internal radiation simulations are performed only for the first 4 meshes due to prohibitive computational costs for higher-density mesh. The temperatures at the midpoint on the lower face are plotted for these different meshes in Figs. 5 and 6, and the estimated order of accuracy is shown in Figs. 7 and 8. The order of accuracy is calculated based on the assumed dependence of discretization error e on the mesh size h

$$e = Ch^k \tag{75}$$

where C is a constant and k is the order of accuracy. The logarithm of ratio of this error for two different mesh sizes is

$$\ell_n\left(\frac{e_1}{e_2}\right) = k\,\ell_n\left(\frac{h_1}{h_2}\right) \tag{76}$$

Equation (76) is used to obtain the order of accuracy, and the result is shown in Figs. 7 and 8. The results from the finest grid are used as the basis to calculate the discretization error. The observed order of accuracy from the results is 2.

A shape design variable studied for this example is the height of face ABCD (see Fig. 4), which is varied through the thickness-to-chord ratio of the cavity at face ABCD. Figure 9 shows a parametric plot of temperature at nodes 1 and 59 for two different cases: 1) both external and internal radiation, with temperature-dependent material properties and 2) only external radiation, with temperature-dependent material properties. Node 1 is on the corner of the cavity and node 59 is the node of maximum temperature at the center of the lower surface on which the heat load is acting. Internal radiation results in lowering the maximum temperature by about 25°C.

Sensitivity analysis is performed at a design variable value of 0.4 and is used to create direct approximations of the temperature, as shown in Fig. 10 for the first case. The direct approximations appear as straight lines tangent to the lines of parametric results obtained by full-order analysis. They verify the accuracy of the sensitivity-analysis formulation presented earlier (both external and internal radiation).

Table 5 Analysis times for wing box (1.83 GHz Intel Core Duo, 1.5 GB DDR2 SDRAM@667 MHz running Mac OSX)

No. of radiation surfaces	$[F_{i-j}]$ time	$[A][B]^{-1}$ time	Total radiation analysis time	Total analysis time	CPU time saved
		Exact analysis			
160	9.92	2980.08	5543.52	10,822.10	——
		$[A][B]^{-1}$ *approximation with 1 term*			
160	9.92	607.32	2838.09	8227.24	2563.44 (23.69%)

Figures 11 and 12 show the temperature results from approximation of $[A][B]^{-1}$ presented in the previous section. The plots are shown for different numbers of terms in the Taylor series expansion in Eq. (68). The approximations were reinitialized every 20 nonlinear iterations. Using zero terms in the Taylor series is equivalent to keeping the $[A][B]^{-1}$ factor (calculated at the beginning of nonlinear iterations) as constant throughout the solution of the system. For a number of terms greater than 0, this factor is updated per iteration and hence leads to greater accuracy for calculation of both temperature and its sensitivity. The savings in CPU cost for approximation with 1 term is presented in Table 3, which shows as much as a 53% reduction in CPU cost.

Wing Box

A wing box under thermal loading has been analyzed and the results are verified against NASTRAN. Transient analysis was performed with temperature-dependent material properties. Load cases with and without internal radiation were analyzed. Design-oriented-analysis results for constant (temperature-independent) material properties and a steady-state case were presented in part 1 [1]. The material properties [9] used for this case are shown in Table 1, and their variation with temperature is shown in Figs. 2 and 3.

The wing box has a total of 4 spar webs and 8 rib webs; together, they form 21 internal cavities that are participating in heat transfer through internal cavity radiation. The upper and lower surfaces of the wing box have a layer of thermal protection system (TPS) and a uniform heat flux of 80 and 1 $\mathrm{kW/m^2}$, respectively, and they are radiating externally. This, together with conduction heat transfer in the structure, defines the thermal analysis case for the wing box, which is transient in nature. The transient analysis is performed for a total of 3000 s using an implicit Newmark scheme with 1 s time steps. Results (including sensitivities) are presented for a point in time of $t = 3000$ s.

Figure 13 shows a sample finite element mesh used for the analysis. The configuration geometry shape design variables used for creating the wing-box geometry are listed in Table 4, and the mesh shown in this figure has 2638 nodes and 5696 elements. Because of the nonlinear dependence of temperature properties on temperature, it is important to have a sufficient number of elements in the thickness direction of the TPS. The effect of the number of elements in the thickness direction is shown in Fig. 14. A mesh convergence study is performed for the number of elements in the wing-box finite element mesh, and the results presented in this paper are from a mesh with converged temperature results.

Figure 15 shows the variation of temperature on nodes 1 and 37 on the lower skin for various loading conditions for both constant and temperature-dependent material properties. Node 1 is located at the root leading edge, and node 37 is located between the first and second ribs from the root and between the first and second spars from the leading edge. The maximum temperature on the wing occurs at this node.

The important aspects to be noted in Fig. 15 are that the effect of temperature dependence of material properties is very substantial and that internal radiation leads to a reduction of maximum temperature observed on the wing by about 15%. The temperature plot of both nodes 1 and 37 for constant (temperature-independent) material properties for the cases with and without internal radiation lie very close to each other. This is because of the dependence of internal radiation on the fourth power of temperature, the effect of which becomes more pronounced at higher temperatures.

Figures 16–18 show comparisons of results from the FESystem (the newly developed design-oriented analysis capability) and NASTRAN. Figures 19–22 show sensitivity-analysis results for the different cases. All direct approximation lines are tangent to the full-order analysis, thereby validating the sensitivity-analysis formulation.

Figure 23 shows the temperature calculation from approximation of $[A][B]^{-1}$ presented in the previous section. As in the case of the simple cavity, the plots are shown for different numbers of terms in the Taylor series expansion in Eq. (68). Using one or more terms in the approximation results in greater accuracy for calculation of both temperature and its sensitivity. The savings in CPU cost for approximation with one term is presented in Table 5, which shows a 23% reduction in CPU cost.

Conclusions

For aerospace structures operating in extreme thermal environments, material properties become dependent on the temperatures in the structure, and multiple modes of heat transfer have to be taken into account. In a previous publication [1], the authors introduced shape sensitivity analysis of problems with internal cavity radiation for steady-state problems and temperature-independent material properties. The present paper presents the formulation for transient thermal analysis with temperature-dependent material properties. The computational challenges for the given problem are identified and a new approximation scheme is proposed to reduce associated high CPU costs. Analysis, sensitivity, and approximation results presented in the paper verify the formulation and show the computational advantage for both steady-state and transient heat transfer problems with temperature-dependent material properties. The focus in the present paper has been on the conduction–radiation problem. Integration of conduction–radiation modeling with structural analysis has already been discussed in [1].

Acknowledgments

This work was supported by NASA as part of the Space Vehicle Technology Institute (SVTI) and the Constellation University Institutes Project (CUIP). We are grateful for this support.

References

[1] Bhatia, M., and Livne, E., "Design-Oriented Thermostructural Analysis with External and Internal Radiation, Part 1: Steady State," *AIAA Journal*, Vol. 46, No. 3, 2008, pp. 578–590. doi:10.2514/1.26236

[2] Bhatia, M., and Livne, E., "Thermal Vibration and Sensitivity Analysis for Shape Optimization of Thin Walled Aerospace Structures," AIAA Paper 2007-2125, 2007.

[3] Dems, K., and Korycki, R., "Sensitivity Analysis and Optimum Design for Steady Conduction Problem with Radiative Heat Transfer," *Journal of Thermal Stresses*, Vol. 28, No. 2, 2005, pp. 213–232. doi:10.1080/014957390900166

[4] Korycki, R., "Sensitivity Analysis and Shape Optimization for Transient Heat Conduction with Radiation," *International Journal of Heat and Mass Transfer*, Vol. 49, No. 13–14, 2006, pp. 2033–2043. doi:10.1016/j.ijheatmasstransfer.2006.01.007

[5] Thornton, E. A., *Thermal Structures for Aerospace Applications*, AIAA, Reston, VA, 1996.

[6] Bathe, K. J., *Finite Element Procedures*, Prentice–Hall, Englewood Cliffs, NJ, 1996.

[7] Haftka, R. T., and Gurdal, Z., *Elements of Structural Optimization*, 3rd ed., Kluwer Academic, Norwell, MA, 1992.

[8] Bae, H.-R., Grandhi, R. V., and Canfield, R. A., "Successive Matrix Inversion Method for Reanalysis of Engineering Structural Systems," *AIAA Journal*, Vol. 42, No. 8, 2004, pp. 1529–1535. doi:10.2514/1.4715

[9] Williams, S., and Curry, D., "Thermal Protection Materials," NASA, Ref. Publ. 1289, 1992.

T. Zang
Associate Editor